Article

Modulation of Cell-Cycle Progression by Hydrogen Peroxide-Mediated Cross-Linking and Degradation of Cell-Adhesive Hydrogels

Wildan Mubarok [†] , Kelum Chamara Manoj Lakmal Elvitigala [†], Masaki Nakahata , Masaru Kojima and Shinji Sakai *

Department of Materials Engineering Science, Graduate School of Engineering Science, Osaka University, Toyonaka 560-8531, Osaka, Japan; wildanmubarok@cheng.es.osaka-u.ac.jp (W.M.); kelum@cheng.es.osaka-u.ac.jp (K.C.M.L.E.); nakahata@cheng.es.osaka-u.ac.jp (M.N.); kojima@cheng.es.osaka-u.ac.jp (M.K.)
* Correspondence: sakai.shinji.es@osaka-u.ac.jp; Tel.: +81-6-6850-6252
† These authors contributed equally to this work.

Abstract: The cell cycle is known to be regulated by features such as the mechanical properties of the surrounding environment and interaction of cells with the adhering substrates. Here, we investigated the possibility of regulating cell-cycle progression of the cells on gelatin/hyaluronic acid composite hydrogels obtained through hydrogen peroxide (H_2O_2)-mediated cross-linking and degradation of the polymers by varying the exposure time to H_2O_2 contained in the air. The stiffness of the hydrogel varied with the exposure time. Human cervical cancer cells (HeLa) and mouse mammary gland epithelial cells (NMuMG) expressing cell-cycle reporter Fucci2 showed the exposure-time-dependent different cell-cycle progressions on the hydrogels. Although HeLa/Fucci2 cells cultured on the soft hydrogel (Young's modulus: 0.20 and 0.40 kPa) obtained through 15 min and 120 min of the H_2O_2 exposure showed a G2/M-phase arrest, NMuMG cells showed a G1-phase arrest. Additionally, the cell-cycle progression of NMuMG cells was not only governed by the hydrogel stiffness, but also by the low-molecular-weight HA resulting from H_2O_2-mediated degradation. These results indicate that H_2O_2-mediated cross-linking and degradation of gelatin/hyaluronic acid composite hydrogel could be used to control the cell adhesion and cell-cycle progression.

Keywords: gelatin; hyaluronic acid; Fucci2; horseradish peroxidase; degradation

1. Introduction

The cell cycle is an intricate process for cell growth. Regulation of the cell cycle is fundamental to successful cell culture technology and tissue engineering. Additionally, dysregulation of the cell cycle is a hallmark of cancer cells, thus, cell-cycle modulation of cancer cells has been a target for developing anticancer drugs [1,2].

In the cellular microenvironment, physical cues including mechanical properties of the substrate and biochemical cues in the form of cell-adhesive ligands are known to modulate cellular behaviors including adhesion [3,4] and proliferation [5–7]. Gelatin and hyaluronic acid (HA) are abundantly found in various tissues of humans and animals [8–10], and are important biomaterials that facilitate strong biological activities [11–13]. The scaffolds composed of multiple polymers provide the microenvironment with multiple properties, attributed to each polymer. For example, gelatin/HA mixture could combine the cell-adhesive property of the arginine–glycine–aspartic acid (RGD) sequence and degradability of the gelatin with the physicochemical property and regulation of cell behavior and immune response function of HA. Therefore, various studies have reported the usefulness of gelatin/HA composite hydrogel scaffolds in tissue-engineering applications for biomimicking of the extracellular matrix (ECM) of the native tissues [10,14–16].

The biological activities of HA are related to its molecular weight. High-molecular weight HA is required for wound healing [17], while low-molecular-weight fragments of HA act as an activator of dendritic cells and macrophages during inflammation [18,19]. More importantly, the molecular weight of HA also governs oncogenesis: high-molecular-weight HA inhibits the progression of tumor growth, while low-molecular-weight HA has an opposing effect [20–22].

Hydrogen peroxide (H_2O_2) is widely used for degrading high-molecular-weight HA, gelatin, and various other polymers, through oxidative cleavage of the bonds [23–26]. Apart from polymer degradation, H_2O_2 is also used as an electron donor of horseradish peroxidase (HRP)-mediated reaction resulting in gelation of aqueous solutions of polymers with phenolic hydroxyl groups (Polymer–Ph), including Gelatin–Ph and HA–Ph. The hydrogelation through HRP-mediated cross-linking has been applied for a variety of biomedical applications, e.g., cell transplantation [27], bone regeneration [28], wound dressing [29], and inks for 3D bioprinting [30]. In the applications of using H_2O_2 for inducing HRP-mediated hydrogelation, no attention has been paid to the contradictory functions of H_2O_2 for inducing the degradation of the polymers. Recently, we reported that the contradictory function of H_2O_2 affects the mechanical property of hydrogels, which leads to changes in adhesion of the human adipose-derived stem cells (hASCs) and rat fibroblast cells [31]. However, the contradictory effect of H_2O_2 on other cell behaviors, such as cell-cycle progression, has not been investigated.

Cell-cycle modulation by the physical microenvironment of the cells has recently garnered great interest [32,33]. Although previous studies have reported the cell-cycle modulation by HA in collagen matrix [34], methacrylated gelatin [35], and chitosan–gelatin complex [36], no studies have investigated the cell-cycle modulation by Gelatin–Ph/HA–Ph composite hydrogel. This is particularly important considering that Gelatin and HA are known to be the component of the cancer microenvironment [33,37]. Therefore, in this study, we aimed to investigate the effect of H_2O_2 as an electron donor in HRP-mediated cross-linking and degradation-inducing oxidant of Gelatin–Ph/HA–Ph composite hydrogels on the cell-cycle progression (Figure 1).
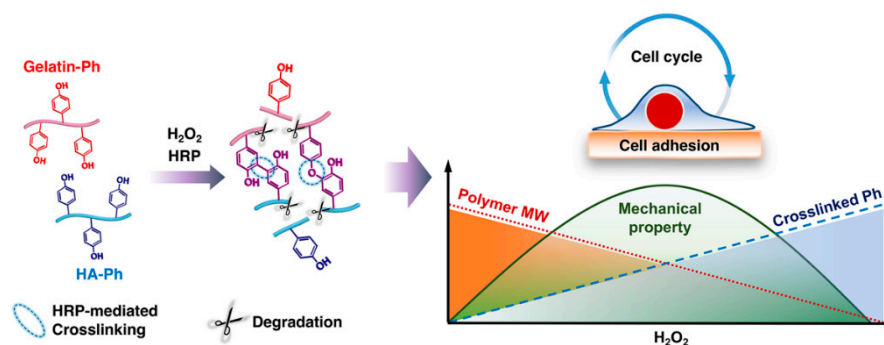
Figure 1. Schematic illustration of H_2O_2-mediated hydrogelation of Gelatin–Ph/hyaluronic acid (HA)–Ph composite through horseradish peroxidase (HRP)–mediated cross-linking of Ph moieties and polymer degradation, and its subsequent effect on cell adhesion and the cell cycle.

In this study, we focused on the cell-cycle progression of cervical cancer cells, due to its high clinical prevalence worldwide, and being one of the highest causes of death in low-income countries [38]. Additionally, there is an effort to accelerate the cervical cancer elimination worldwide [39]. Hydrogel itself, including hyaluronic acid and gelatin, has been applied to tumor sites following tumor removal surgery to prevent tumor recurrence [40,41]. Here, we studied the cell-cycle progression of human cervical cancer cells using HeLa cells expressing genetically encoded fluorescent ubiquitylation-based cell-cycle indicator FucciHeLa cell is selected since it has been extensively used in biomedical study and research on cell-cycle regulation [42], while HeLa/Fucci2 cell has been used to study cell response following drug-induced cell-cycle arrest [43]. Fucci2 is composed of two chimeric

fluorescent proteins, mCherry-hCdt1 and mVenus-hGem. Reciprocal accumulation of these two proteins turns cell nuclei red-fluorescent in G1 phase and green-fluorescent in the S/G2/M phases.

Additionally, we also investigated the cell-cycle progression of non-transformed mouse mammary gland epithelial cell line (NMuMG) expressing FucciNMuMG is widely used to study the epithelial-to-mesenchymal transition (EMT), a physiological change that is necessary for cancer invasion and metastasis [44,45]. In addition, previous study has reported that HeLa/Fucci2 and NMuMG/Fucci2 have different cell-cycle response following chemical treatment [43]. Therefore, we studied both the HeLa/Fucci2 and NMuMG/Fucci2 cell cycle to investigate whether cell type-specific phenomenon also occurs when cultured on Gelatin–Ph/HA–Ph composite hydrogel with different physicochemical properties.

2. Materials and Methods

2.1. Materials

Gelatin (Type B; ca. 225 g bloom, bovine skin) was purchased from Sigma–Aldrich (St. Louis, MO, USA). Sodium hyaluronate (HA, MW ~1000 kDa) was purchased from Kewpie (Tokyo, Japan). Horseradish peroxidase (HRP, 140 U/mg), *N*-hydroxysuccinimide (NHS), *N*,*N*-dimethylformamide (DMF), hydrogen peroxide (H_2O_2) aqueous solution (31 *w/w*%), and catalase from bovine liver were purchased from Wako Pure Chemical Industries (Osaka, Japan). Water-soluble carbodiimide hydrochloride (WSCD·HCl) was obtained from Peptide Institute (Osaka, Japan). List of abbreviations used in this article is provided in Table 1.

Table 1. List of abbreviations. The abbreviations are reported alphabetically.

Abbreviation	Full Form
CLSM	Confocal laser-scanning microscope
DMEM	Dulbecco's Modified Eagle Medium
DMF	*N*,*N*-dimethylformamide
ECM	Extracellular matrix
EGF	Epidermal growth factor
EMT	Epithelial-to-mesenchymal transition
FBS	Fetal bovine serum
Fucci	Fluorescent ubiquitination-based cell-cycle indicator
HA	Hyaluronic acid
hASCs	Human adipose-derived stem cells
HEPES	4-(2-hydroxyethyl)-1-piperazineethanesulfonic acid
HRP	Horseradish peroxidase
LMW-HA	Low-molecular-weight hyaluronic acid
MW	Molecular weight
NHS	*N*-hydroxysuccinimide
PBS	Phosphate buffered saline
PFA	Paraformaldehyde
Ph	Phenolic hydroxyl moieties
PI	Propidium iodide
RGD	Tripeptide arginine–glycine–aspartic acid
RHAMM	Receptor for hyaluronic acid-mediated motility
WSCD·HCl	Water-soluble carbodiimide hydrochloride

2.2. Polymer–Ph Preparation

Gelatin–Ph (1.9×10^{-4} mol-Ph/g-Gelatin–Ph) and HA–Ph (1.5×10^{-4} mol-Ph/g-HA–Ph) were prepared by conjugating 3-(4-hydroxyphenyl) propionic acid with gelatin and tyramine hydrochloride with HA, respectively, using WSCD·HCl/NHS as previously reported [46,47].

2.3. Cell Culture

HeLa/Fucci2 and NMuMG/Fucci2 cell lines were obtained from RIKEN Bio-Resource Center (Ibaraki, Japan). HeLa/Fucci2 was cultured in Dulbecco's Modified Eagle Medium

(DMEM, Nissui, Tokyo, Japan) containing 10 $v/v\%$ fetal bovine serum (FBS). NMuMG/Fucci2 was cultured in DMEM supplied with 10 $v/v\%$ FBS and 10 µg/mL insulin (Sigma, St. Louis, MO, USA) [43]. Cells were cultured at 37 °C in a 5% CO_2 incubator.

2.4. Hydrogel Mechanical Properties Measurement

An aqueous solution (600 µL/well) containing 3.0 $w/v\%$ Gelatin–Ph, 0.5 $w/v\%$ HA–Ph, and 1 U/mL HRP was poured into a well of 12-well plate. The well-plate was then put into a plastic box (13.5 cm × 9.5 cm × 7 cm) and exposed to air containing H_2O_2 for 15, 30, 45, 60, 90, and 120 min. The air containing H_2O_2 was prepared by bubbling air into a solution containing 1 M H_2OConcentration of the air containing H_2O_2 was measured at 16 ppm using gas detector (C-16 PortaSense II, Analytical Technology, Inc., Collegeville, PA, USA). The Young's moduli of the resultant Gelatin–Ph/HA–Ph composite hydrogels were measured using a material tester (EZ-Test, Shimadzu, Kyoto, Japan) by compressing the hydrogels with a probe (diameter, 8 mm) at a compression rate of 6.0 mm/min. The Young's modulus was calculated from the data obtained in the range 1–10% compression strain (Figure S1).

2.5. Cell Adhesion and Cell-Cycle Analysis

Hydrogel sheets were fabricated from PBS solution containing 3.0 $w/v\%$ Gelatin–Ph, 0.5 $w/v\%$ HA–Ph, and 1 U/mL HRP. The solution was added to a 12-well plate at 600 µL/well and exposed to air containing 16 ppm H_2O_2 for 15, 60, and 120 min. One milliliter culture medium containing 1 mg/mL catalase was then layered on the fabricated hydrogels overnight to degrade the remaining H_2O_2 into H_2O and OThe cell cycle was synchronized to S-phase by incubating the cells in medium containing 4 mM hydroxyurea for 24 h [48]. After the synchronization, cells were trypsinized and seeded on the fabricated gel sheet at 1.0×10^4 cells/well (2.6×10^3 cells/cm^2). The cell cycle was observed at 1 and 2 days after seeding based on the fluorescence expression of the mCherry-hCdt1 (red) and mVenus-hGem (green) of the Fucci2, using fluorescence microscope (BZ-9000, Keyence, Tokyo, Japan). Red fluorescence indicates G1, yellow indicates G1/S, and green indicates late S/G2/M phase (Figure S2). The number of cells on each phase was counted using ImageJ (2.1.0/1.53c, NIH, Bethesda, MD, USA) from 5–10 randomly selected areas. For live imaging, cells were observed using confocal laser-scanning microscope (CLSM, C2; Nikon, Tokyo, Japan). The 12-well plate containing cells on fabricated hydrogel were placed in a stage-top incubator (STXG-WSKMX; Tokai Hit, Shizuoka, Japan) set at 37 °C supplied with 5% CO_2 + 20% O_2 + NTime-lapses were conducted for 48 h. Cell adhesion analysis was conducted by analyzing the morphology of the cells including cell area, perimeter, aspect ratio, and circularity of more than 50 cells for each set of conditions using ImageJ. Aspect ratio was defined as the ratio between major axis/minor axis of the fitted ellipse. Circularity was calculated using the formula: 4π (area/perimeter^2). Higher aspect ratio indicates elongated morphology. Higher circularity value (near 1.0) indicates a circular shape.

2.6. Viability Analysis

Viability of the cells was analyzed by staining the cells with Calcein–AM (Nacalai Tesque Inc., Kyoto, Japan) and propidium iodide (PI, Cellstain®, Dojindo, Kumamoto, Japan). Cells were incubated with PBS solution containing 3.3 µg/mL Calcein–AM and PI for 10 min at 37 °C. Live cells stained with Calcein–AM and dead cells stained with PI were observed using fluorescence microscope. Number of viable and dead cells were counted using ImageJ from micrographs taken on 6 randomly selected areas. Viability was calculated as percentage of number of live cells/total number of cells.

2.7. F-Actin Analysis

F-actin of the cells was stained with CytoPainter Phalloidin–iFluor 488 Reagent (ab176753, Abcam, Cambridge, UK). Briefly, cells were fixed with 4% paraformaldehyde

(PFA) in PBS, permeabilized in HEPES (4-(2-hydroxyethyl)-1-piperazineethanesulfonic acid)-buffered solution (pH 5.5), and stained with CytoPainter Phalloidin–iFluor 488 Reagent (1X) according to the manufacturer's protocol. The number of cells with stress fibers was counted using ImageJ based on the presence/absence of visible stress fibers (Figure S3). F-actin fluorescence intensity was measured using ImageJ by measuring integrated density defined as sums of all the intensity in the pixel of the selected areas.

2.8. Statistical Analysis

Data were statistically analyzed using Microsoft® Excel® 2019 (Version 1808, Microsoft Corp., Redmond, WA, USA). Statistical analysis was conducted using one-way analysis of variance (ANOVA) followed by post hoc *t*-test using Tukey HSD. Data were considered significantly different if $p < 0.05$.

3. Results

3.1. Mechanical Properties

First, the effect of H_2O_2 exposure time (15–120 min) on the stiffness of Gelatin–Ph/HA–Ph composite hydrogels was investigated by measuring the Young's modulus. Using this setup, hydrogel could be fabricated within 40 s (Figure S4). The result obtained from this experiment showed that H_2O_2 exposure time governed the Young's modulus of the composite hydrogels ($p < 0.005$) (Figure 2). The Young's modulus of the hydrogels increased as the exposure time to H_2O_2 was extended to 45 min, from 0.20 ± 0.01 kPa and 0.20 ± 0.03 kPa at 15 and 30 min of the exposure, respectively, to 0.44 ± 0.02 kPa at 45 min of the exposure. Extending the exposure time to 60 min resulted in the hydrogel with the highest Young's modulus of 1.27 ± 0.30 kPa. Prolonging the exposure time to 90 and 120 min, however, resulted in the decrease of Young's modulus to 0.41 ± 0.05 kPa and 0.40 ± 0.04 kPa, respectively (Figure 2).
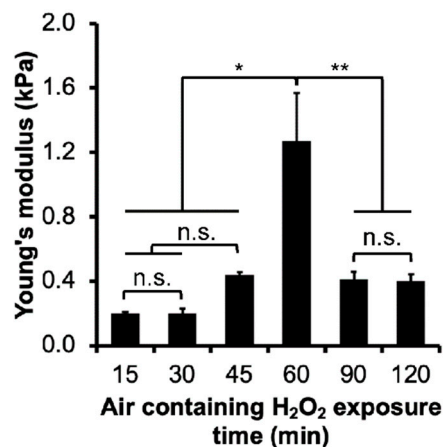
Figure 2. Effect of exposure time to H_2O_2 on the Young's modulus of Gelatin–Ph/HA–Ph composite hydrogels obtained from 3.0 *w/v*% Gelatin–Ph, 0.5 *w/v*% HA–Ph, and 1 U/mL HRP. Values: Mean $\pm$ SE ($n = 3$). * $p < 0.05$, ** $p < 0.005$, n.s.: no significant difference ($p > 0.05$), Tukey HSD.

3.2. HeLa/Fucci2 Adhesion

Next, the effect of the exposure time to H_2O_2 (15, 60, and 120 min) on the adhesion of the HeLa/Fucci2 cells on the resultant composite hydrogels was investigated. The content of Gelatin–Ph (3.0 *w/v*%) and HA–Ph (0.5 *w/v*%) in the composite hydrogels used in this study has been reported to allow the elongation of hASCs and support the growth of the cells [49]. As for the exposure time, 15, 60, and 120 min were selected since the Young's moduli of the composite hydrogels obtained through 15 min (0.20 kPa) and 120 min (0.40 kPa) of H_2O_2 exposure were relatively similar. Meanwhile, hydrogel obtained through 60 min of the exposure had the highest Young's modulus of 1.27 kPa (Figure 2).

First, the viability of the HeLa/Fucci2 cells cultured on the hydrogel was investigated. Viability of the cells was determined by staining the cells with Calcein–AM (green) and PI (red) that stained live and dead cells, respectively (Figure S5). Viability analysis showed that HeLa/Fucci2 cells had high viability ($\geq$85%) from day 1 to day 2 of culture on the hydrogel, independent of the H_2O_2 exposure time (Figure 3a).
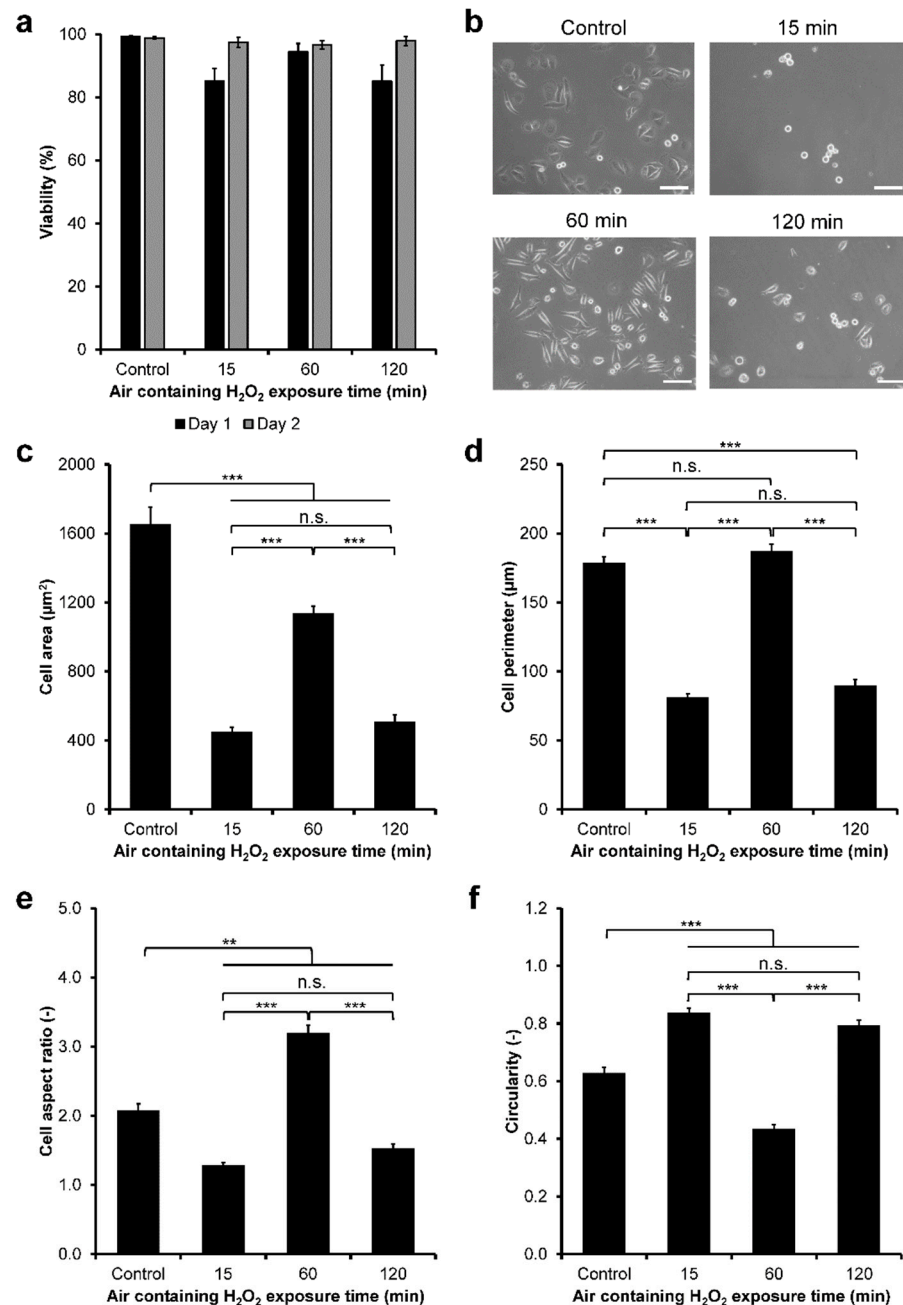
Figure 3. Viability and morphology of HeLa/Fucci2 cell on Gelatin–Ph/HA–Ph composite hydrogels obtained through different exposure time to H_2O_2. (**a**) Viability of HeLa/Fucci2 cells calculated based on Calcein–AM/PI staining. Bar: S.E. (*n* = 6) (**b**) Micrograph of HeLa/Fucci2 cells on the composite hydrogels after 1 day cultured on well-plate (control) and the hydrogels obtained through 15, 60, and 120 min exposure to H_2OScale bars: 100 μm. (**c**) Area, (**d**) perimeter, (**e**) aspect ratio, and (**f**) circularity of HeLa/Fucci2 cells. Bar: S.E. (*n* > 100 cells). ** *p* < 0.005, *** *p* < 0.0005, n.s.: no significant difference (*p* > 0.05) based on Tukey HSD.

Next, HeLa/Fucci2 cell adhesion was investigated by analyzing the morphology of the cells. HeLa/Fucci2 cells had different morphology on the hydrogels (Figure 3b). The cells cultured on the hydrogels obtained through 15 min and 120 min exposure to H_2O_2 showed no significant difference ($p > 0.05$) in the cell area (Figure 3c), perimeter (Figure 3d), aspect ratio (Figure 3e), and circularity (Figure 3f). These cells appeared to be small and circular indicated by the smallest area and perimeter, lowest aspect ratio, as well as the highest circularity. Meanwhile, the cells cultured on the hydrogel obtained through 60 min of exposure to H_2O_2 showed the larger area and perimeter, highest aspect ratio, and the lowest circularity, indicating large and elongated morphology, relatively similar to those on cell culture dish (control, Figure 3b–f).

3.3. HeLa/Fucci2 Cell-Cycle Progression

Next, the cell-cycle progression of HeLa/Fucci2 cells was investigated. Fucci2 allows observation of the expression of mCherry-hCdt1 (red) and mVenus-hGem (green), observed at G1 and S/G2/M, respectively. G1/S transition could be observed as yellow fluorescence (Figure S2). Before seeding, the cell cycle was synchronized with hydroxyurea. After 24 h of 4 mM hydroxyurea exposure, HeLa/Fucci2 predominantly found in S-phase, shown as green fluorescence (Figure 4a). The cells were then seeded on the composite hydrogels obtained through the different time of exposure to H_2O_2, and the cell cycle was observed for two days after seeding (Figure 4b).
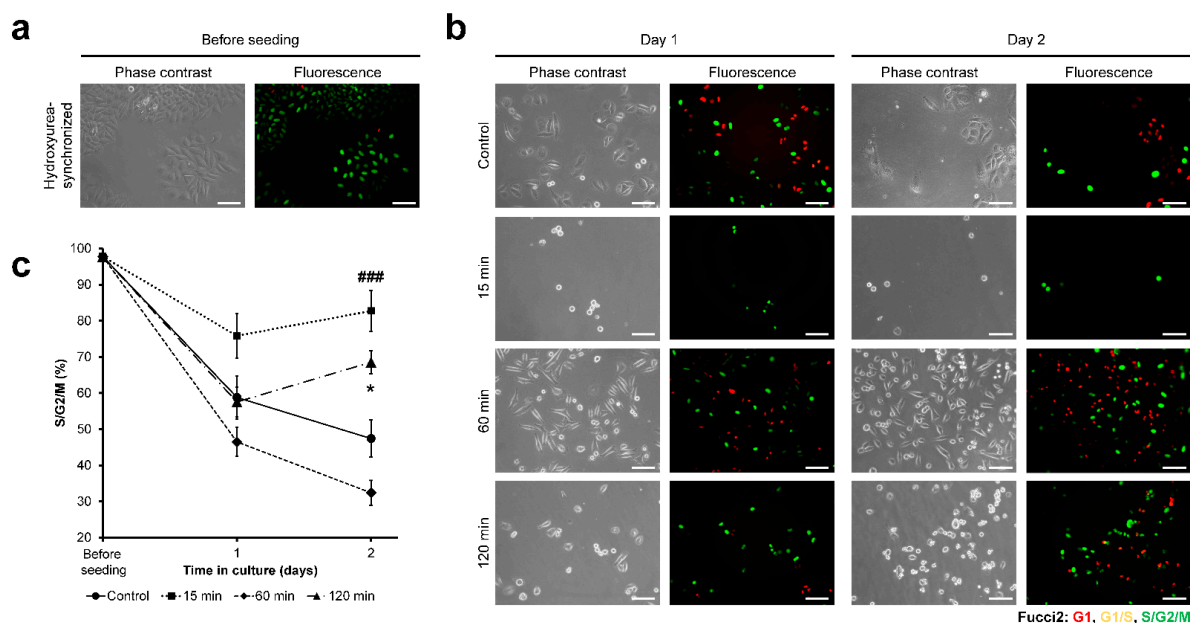
Figure 4. Exposure time to H_2O_2-dependent changes in Gelatin–Ph/HA–Ph composite hydrogel stiffness could modulate the cancer cell-cycle progression. (**a**) Phase-contrast and fluorescence observation of the HeLa/Fucci2 before seeding, showing cell synchronized in S-phase, and (**b**) cells at day 1 to day 2 after seeding on the hydrogels. Cells cultured on well-plate were used as control. Fluorescence expression of Fucci2: red indicates G1, yellow indicates G1/S, and green indicates late S/G2/M phase. Scale bar: 100 μm. (**c**) Percentage of HeLa/Fucci2 cells in S/G2/M phase. Bar: S.E. ($n = 10$). $^{###}$ $p < 0.0005$, 15 min compared to control; * $p < 0.05$, 120 min compared to control, using Tukey HSD.

Cell-cycle analysis shows that the cells on cell culture well-plate (control) showed progression of the cell cycle marked by a continuous decrease in the percentage of cells at S/G2/M phase, from 97.8% before seeding to 58.8% at day 1 and 47.4% at day 2 (Figure 4c). The cells cultured on the hydrogel obtained through 60 min of exposure to H_2O_2 showed a similar trend as those on cell well-plate (control, $p > 0.05$), with a decreasing percentage of

cells at S/G2/M phase, to 32.4% at day 2 after seeding. In contrast, the cells cultured on the hydrogels obtained through 15 and 120 min of the exposure remained at S/G2/M phase, with 82.7% and 68.5% of the cells were found in S/G2/M phase at day 2, respectively (Figure 4c). To further confirm this observation, a live-imaging experiment was conducted by observing the HeLa/Fucci2 cells from 8–48 h post-seeding. Live-imaging observation showed higher mitosis frequency in HeLa/Fucci2 cells cultured on 60 min composite hydrogel and control (Movie S1). Additionally, cell growth was analyzed by calculating the cell density on day 1 and day 2 post-seeding. Cells cultured on hydrogel obtained from 15 and 120 min of the exposure showed no significant growth in cells density from day 1 to day 2 ($p > 0.05$). On the other hand, cells cultured on hydrogel obtained from 60 min exposure time to H_2O_2 and control cultured on well-plate showed a significant increase in cell density ($p < 0.05$) (Figure S7).

3.4. HeLa/Fucci2 F-Actin Reorganization

The difference in cell-cycle progression of the cells cultured on each hydrogel might be mediated by the cytoskeleton reorganization. Therefore, the F-actin of the cells was stained, and the formation of stress fibers was investigated (Figure 5a). Most of the cells cultured on cell culture well-plate (control) and those on the hydrogel obtained through 60 min of exposure to H_2O_2 had stress fibers. However, cells cultured on the hydrogel obtained through 15 and 120 min of the exposure had a significantly lower percentage of cells with stress fibers ($p < 0.0005$) (Figure 5b). A similar trend was observed in F-actin integrated density with cells cultured on the hydrogel obtained through the 60 min of exposure to H_2O_2: the cells had significantly higher integrated density ($p < 0.05$) compared to those on the hydrogel obtained through 15 and 120 min of the exposure to H_2O_2 (Figure 5c).
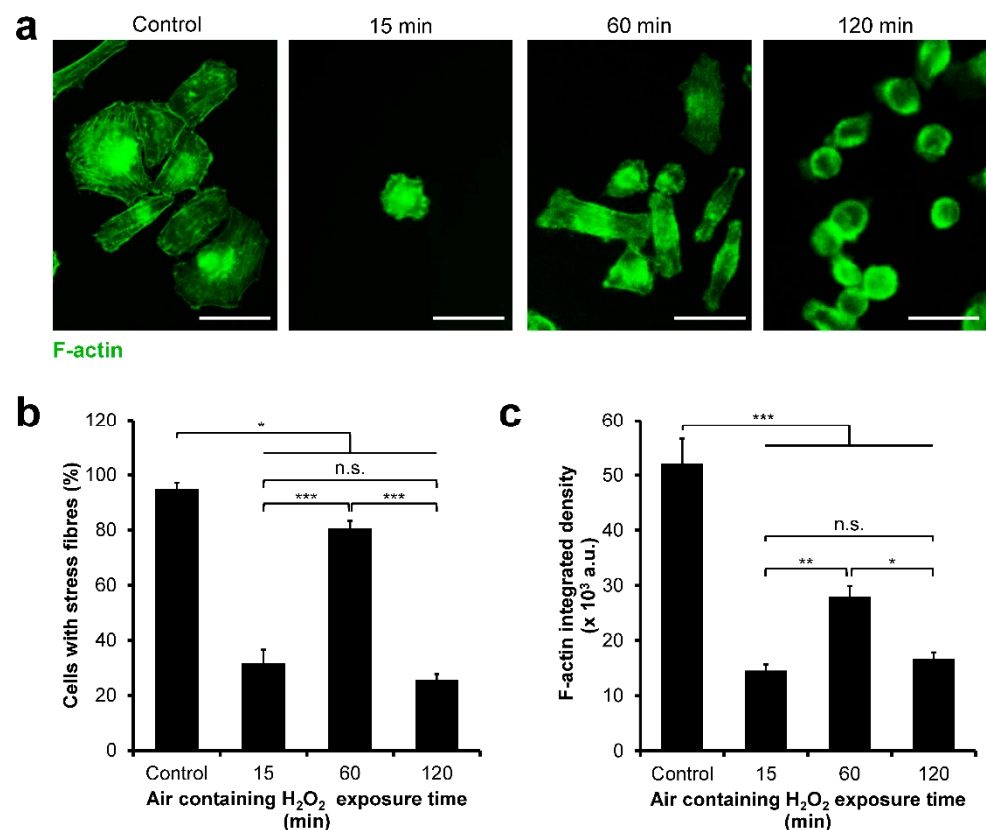
Figure 5. F-actin reorganization in HeLa/Fucci2 cells cultured on Gelatin–Ph/HA–Ph composite hydrogels obtained through 15, 60, and 120 min of exposure to H_2O_2. (**a**) Fluorescence observation of

the F-actin of HeLa/Fucci2 cells cultured on well-plate (control) and the hydrogels. Scale bar: 100 μm. (**b**) Percentage of cells with stress fibers. Bar: S.E. (*n* = 6). (**c**) F-actin integrated density. Bar: S.E. (*n* = 45 cells). * *p* < 0.05, ** *p* < 0.005, *** *p* < 0.0005, n.s.: no significant difference, Tukey HSD.

3.5. NMuMG/Fucci2 Adhesion

Next, the behaviors of NMuMG/Fucci2 cells on the composite hydrogels were investigated. First, the viability of NMuMG/Fucci2 cells on the composite hydrogels was investigated by staining the cells with Calcein–AM/PI (Figure S6). The viability of those NMuMG/Fucci2 cells cultured on the Gelatin–Ph/HA–Ph composite hydrogel was ≥84% (Figure 6a). Additionally, air containing H_2O_2 exposure time did not induce significant changes (*p* > 0.05) in the viability of the NMuMG/Fucci2 cells.
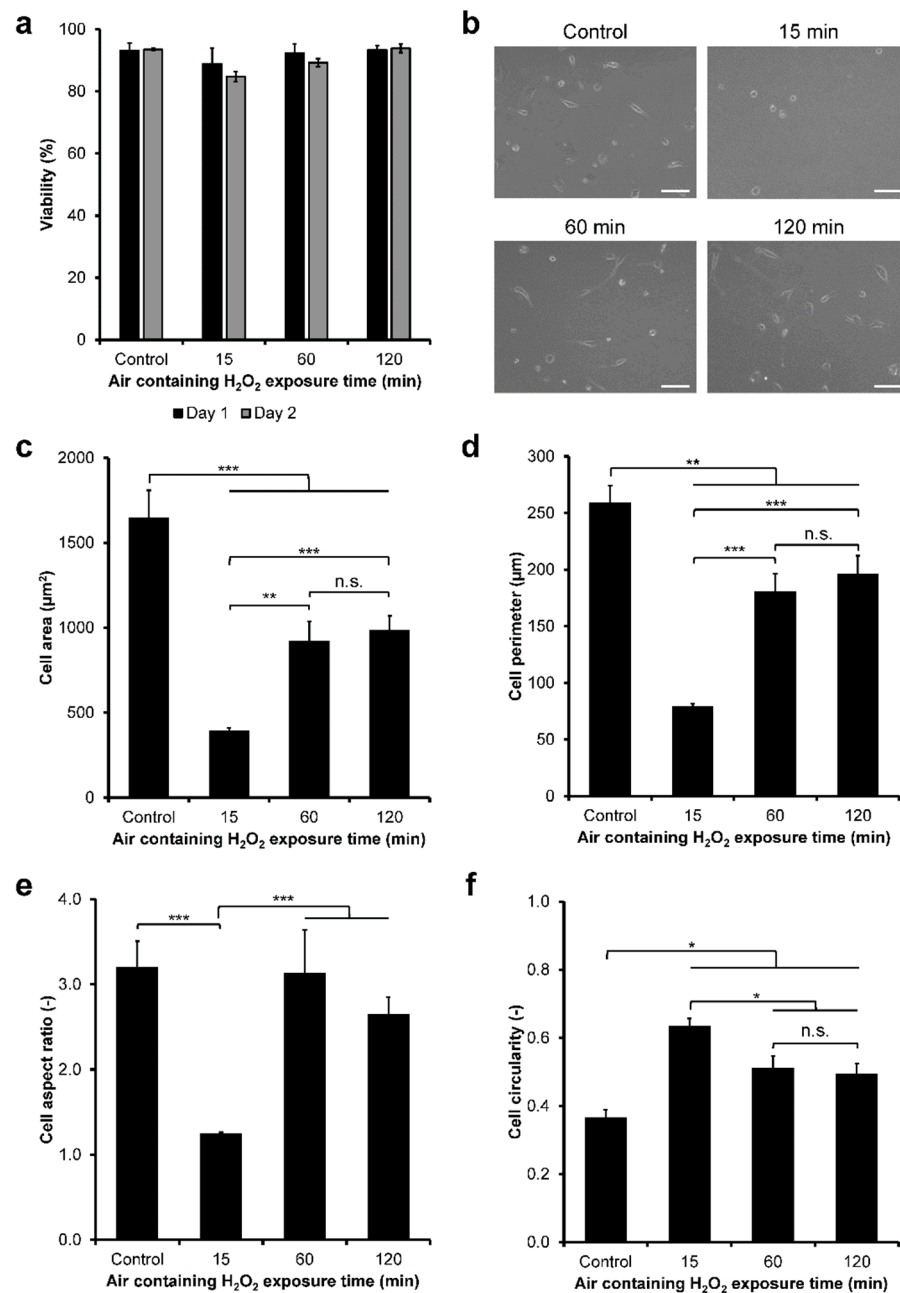
Figure 6. Viability and morphology of NMuMG/Fucci2 cells on Gelatin–Ph/HA–Ph hydrogel

obtained through different exposure time to H_2O_2 in the air. (**a**) Viability of NMuMG/Fucci2 cells on day 1 and day 2 of culture. Bar: S.E. (*n* = 6). (**b**) Representative phase-contrast image of NMuMG/Fucci2 cells on the hydrogels obtained through 15, 60, and 120 min of the exposure. As a control, cells were cultured on plastic surface of the well-plate. Scale bars: 100 μm. (**c**) Area, (**d**) perimeter, (**e**) aspect ratio, and (**f**) circularity of NMuMG/Fucci2 cells. Bar: S.E. (*n* > 50 cells). * *p* < 0.05, ** *p* < 0.005, *** *p* < 0.0005, n.s.: no significant difference, Tukey HSD.

The morphology of the NMuMG/Fucci2 cells on the composite hydrogel was then investigated. The cells on plastic surface of the well-plate (control) and those on the hydrogels obtained through 60 and 120 min of exposure to H_2O_2 elongated similarly (Figure 6b). The cells on the hydrogel obtained through 15 min of the exposure showed a small and round morphology attributed to the smallest area (Figure 6c) and perimeter (Figure 6d), aspect ratio near 1.0 (Figure 6e), and highest circularity (Figure 6f). The cells on the hydrogel obtained through 60 min of the exposure showed significantly larger and elongated shapes attributed to a larger area and perimeter, higher aspect ratio, and lower circularity, compared to cells on hydrogel obtained through 15 min of the exposure. Interestingly, the cells on the hydrogel obtained through 120 min of the exposure had no significant differences (*p* > 0.05) in their morphological characteristics as to those cultured on the hydrogel obtained through 60 min of the exposure.

3.6. NMuMG/Fucci2 Cell-Cycle Progression

Next, the cell-cycle progression of NMuMG/Fucci2 cells on the composite hydrogels was investigated. Hydroxyurea synchronization before seeding resulted in 84.0% S-phase cells (Figure 7a). Cell-cycle observation based on the Fucci2 expression (Figure 7b) showed that the cells on the hydrogels obtained through 15 and 120 min of exposure to H_2O_2 had a significantly higher (*p* < 0.05) percentage of cells at G1 phase from day 1 to day 2 on the hydrogels compared to those on cell well-plate (control) (Figure 7c). In contrast, the percentage of G1-phase cells on the hydrogel obtained through 60 min of the exposure was not significantly different from that of control (*p* > 0.05) (Figure 7c). Time-lapse observation also showed higher mitotic cells in control and those cultured on composite hydrogel obtained from 60 min H_2O_2 exposure time, compared to cells on 15 min and 120 min hydrogel (Movie S2). Cell growth analysis also showed significant cell density increase only in cells cultured on well-plate (control) and 60 min hydrogel (Figure S8).
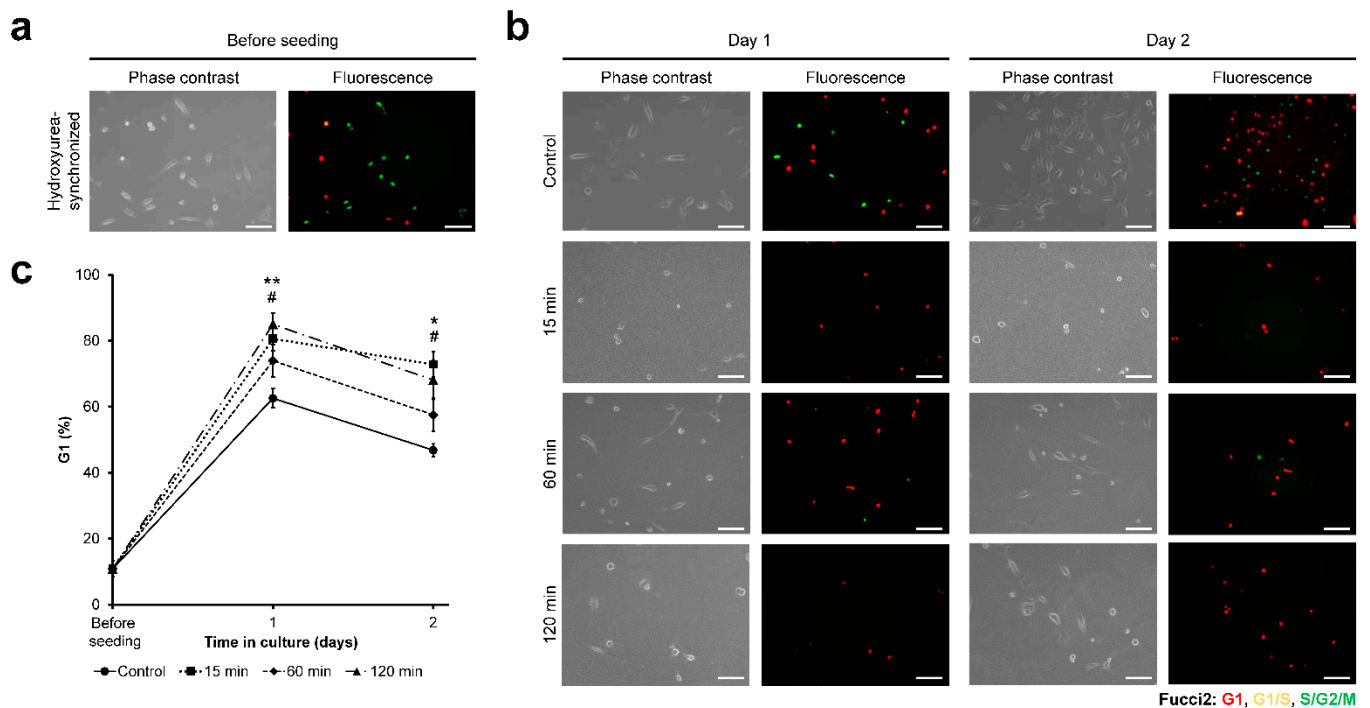
Figure 7. NMuMG/Fucci2 cell-cycle progression on Gelatin–Ph/HA–Ph composite hydrogels obtained through different exposure time to H_2O_2. (**a**) Representative micrograph of NMuMG/Fucci2 cells before seeding, synchronized by hydroxyurea to S-phase, and (**b**) NMuMG/Fucci2 cells on Gelatin–Ph/HA–Ph hydrogel and well-plate (control) for 2 days. Scale bars: 100 μm. (**c**) Percentage of NMuMG/Fucci2 cells in G1 phase. Bar: S.E. ($n \geq 5$). [#] $p < 0.05$, 15 min compared to control; * $p < 0.05$, ** $p < 0.005$, 120 min compared to control, using Tukey HSD.

3.7. NMuMG/Fucci2 F-Actin Reorganization

Next, the F-actin organization of the NMuMG/Fucci2 cells was investigated by staining the actin stress fibers of the cells (Figure 8a). Analysis of the presence of stress fibers showed that the cells cultured on the composite hydrogels obtained through 15 min of exposure to H_2O_2 had the lowest percentage of cells with stress fibers (Figure 8b). Similarly, these cells had the lowest F-actin integrated density (Figure 8c). In contrast, 89.4% of the cells on the hydrogel obtained through 60 min of the exposure had stress fibers, relatively similar to those on cell culture well-plate (control, 96.1%) (Figure 8b) and significantly higher F-actin integrated density ($p < 0.05$) than those on the hydrogel obtained through 15 min of the exposure (Figure 8c). Interestingly, the cells cultured on the hydrogel obtained through 120 min of the exposure had no significant difference ($p > 0.05$) in the presence of actin stress fibers (Figure 8b) and F-actin integrated density (Figure 8c) compared to the cells cultured on the hydrogel obtained through 60 min of exposure to H_2O_2.
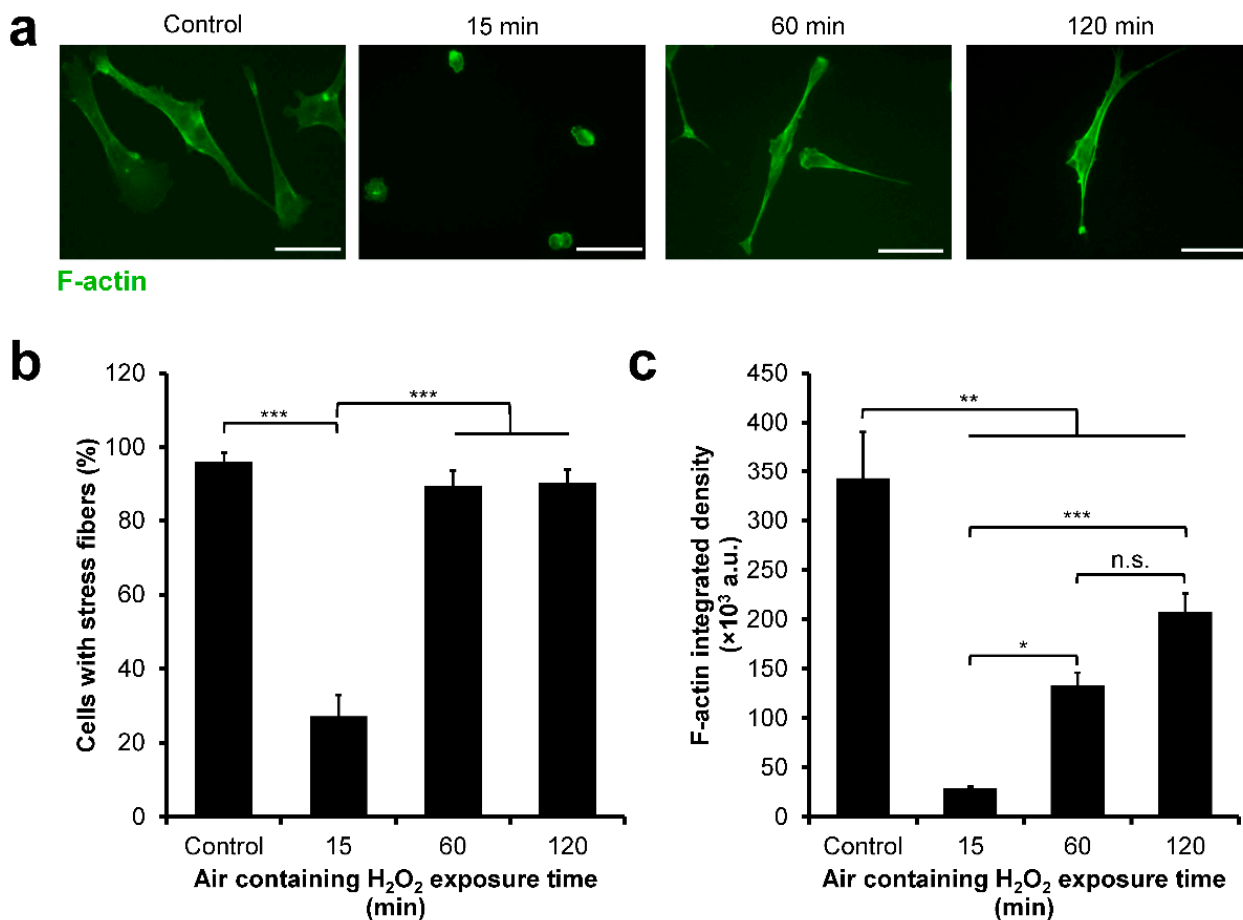
Figure 8. F-actin reorganization of NMuMG/Fucci2 cells cultured on Gelatin–Ph/HA–Ph composite hydrogel obtained through different exposure time to H_2O_2 in the air. (**a**) Representative fluorescence micrograph of the F-actin of NMuMG/Fucci2 cells cultured on Gelatin–Ph/HA–Ph hydrogel obtained through 15–120 min of exposure to H_2OCells cultured on well-plate were used as control. Scale bars: 50 μm. (**b**) Comparison of percentage of cells with stress fibers. Bar: S.E. ($n \geq 5$). (**c**) F-actin integrated density of NMuMG/Fucci2 cells. Bar: S.E. ($n = 50$ cells). * $p < 0.05$, ** $p < 0.005$, *** $p < 0.0005$, n.s.: no significant difference based on Tukey HSD.

4. Discussion

In this study, we aimed to investigate the effect of the contradictory effect of H_2O_2 on the stiffness of Gelatin–Ph/HA–Ph composite hydrogel and its subsequent effect on the modulations of the cell adhesion and cell-cycle progression. Cell-cycle regulation is an important process, particularly with regards to cancer development. Most studies have used anticancer drugs to study the cell-cycle regulation of cancer cells [50,51]. However, few studies have investigated the cancer cell-cycle regulation by the physicochemical properties of their ECM. Here, we used the composite hydrogel to mimic the native ECM environment, which provided a better model for the phenomenon in the native tissues and study for tissue-engineering applications. In this cross-linking system, we used H_2O_2 exposure time to control the mechanical property of the Gelatin–Ph/HA–Ph hydrogels obtained through HRP-mediated cross-linking.

The mechanism of the exposure time-dependent transition of the stiffness of the hydrogels can be explained by the correlation between the degrees of the progress of cross-linking formation catalyzed by HRP, HRP inactivation, and Gelatin–Ph/HA–Ph degradation, which all involve H_2OThe inactivation of HRP [52,53] and degradation of organic molecules including Gelatin and HA by H_2O_2 has been reported [23,54]. In this study, H_2O_2 was supplied continuously to the system containing Gelatin–Ph/HA–Ph and HRP.

Thus, the content of the cross-linked Ph moieties should increase by extending the exposure time to H_2O_2, unless HRP inactivation and Gelatin–Ph/HA–Ph degradation occurred.

Therefore, the results shown in Figure 2 that demonstrate the decrease of Young's modulus with increasing the exposure time from 60 to 120 min, indicate the occurrences of Gelatin–Ph/HA–Ph degradation. Indeed, we confirmed that H_2O_2 could degrade the Gelatin–Ph and HA–Ph polymer, based on the molecular weight measurement (Figure S9). Taken together, a tunable control of Gelatin–Ph/HA–Ph Young's modulus was achieved by simple control of the exposure time to H_2O_2 contained in the air.

Next, we investigated the adhesion and cell-cycle progression of cervical cancer cells using HeLa/Fucci2 cells. Modulation of the cell cycle of cancer cells has garnered great interest to study the progression of tumors and inhibition of tumor growth [1,2]. Changes in the physicochemical properties in ECM as well as cell–ECM adhesion are also known to modulate tumor cells invasion and metastasis [55,56]. First, we investigated the viability of the cells. HeLa/Fucci2 cells showed high viability regardless of the air containing H_2O_2 exposure time (Figure 3a; Figure S5). This result could be attributed to the well-known biocompatibility of both Gelatin–Ph and HA–Ph [49,57,58]. Next, our results showed that HeLa/Fucci2 cells had mechanical property-dependent changes in cell adhesion (Figure 3b–f) and cell-cycle progression (Figure 4). HeLa/Fucci2 cells cultured on soft hydrogel obtained through 15 min (0.20 kPa) and 120 min (0.40 kPa) of H_2O_2 exposure had similar morphology with small size and round shape. Meanwhile, HeLa/Fucci2 cells cultured on stiffer hydrogel (1.27 kPa) obtained through 60 min of the exposure had larger size and elongated morphology (Figure 3b–f). The stiffness-dependent change in cell morphology is consistent with the results of previous studies using hASCs cultured in Gelatin–Ph/HA–Ph hydrogel [49] and fibroblast cells on DNA cross-linked hydrogel, which showed a spherical shape on soft substrates and an elongated shape on stiff substrates [59]. Based on these results, H_2O_2 exposure time-mediated changes to Gelatin–Ph/HA–Ph stiffness could govern the adhesion of HeLa/Fucci2 cells.

As for the cell-cycle progression, we found that stiffer hydrogel is required for HeLa/Fucci2 cell-cycle progression. Cells cultured on soft hydrogel obtained through 15 min and 120 min of exposure to H_2O_2 had an arrested cell cycle at G2/M phase (Figure 4), which resulted in halted cell growth (Figure S7). In contrast, cells on the hydrogel obtained through 60 min of H_2O_2-exposure had similar progression to those of control (Figure 4), which allows cell growth (Figure S7). Our result is consistent with the results reported by Paszek et al. [60]. They reported that cancer cells cultured on soft collagen gel had lower growth and adhesion [60]. Wall et al. reported that melanoma cells cultured in fibrillar collagen had a cell-cycle arrest in G2 [61]. The progression of the cell cycle on stiffer substrates observed in this study is consistent with the results reported by Klein et al. about the cell-cycle progression in stiff polyacrylamide hydrogels, but not in soft hydrogels, after nocodazole-mediated G2/M arrest [62].

The difference in the cell-cycle progression of cells cultured on soft and stiff hydrogel could be attributed to the F-actin assembly. Previous studies have reported that actin plays a key role in mitosis [63,64]. Indeed, we found that HeLa/Fucci2 cells had lower F-actin assembly on soft hydrogel obtained through 15 min (0.20 kPa) and 120 min (0.40 kPa) of H_2O_2 exposure (Figure 5). Previous studies have reported that actin disruption could lead to G2/M arrest in transformed cancer cell line IMR-90 and MCF-7 cells [65,66]. Accordingly, cells cultured on composite hydrogel obtained through 15 min and 120 min of H_2O_2 exposure that showed a reduction in stress fibers assembly (Figure 5) also showed G2/M arrest (Figure 4). This indicates that one of the possible causes of cell-cycle arrest at G2/M phase observed in the HeLa/Fucci2 cells cultured on soft hydrogel obtained through 15 min and 120 min of exposure to H_2O_2 is due to the reduction in stress fibers assembly.

Next, the adhesion and cell-cycle progression of NMuMG/Fucci2 cells was investigated. Similar to the result in HeLa/Fucci2 cells, NMuMG/Fucci2 cells showed high viability from day 1 to day 2 on the Gelatin–Ph/HA–Ph composite hydrogel, independent of the H_2O_2 exposure time (Figure 6a; Figure S6). Interestingly, we found some responses

in NMuMG/Fucci2 cells that differ from HeLa/Fucci2 cells. Cell morphology analysis showed that while NMuMG/Fucci2 cells also had small and round morphology on the hydrogel obtained through 15 min of exposure to H_2O_2, cells cultured on the hydrogel obtained through 120 min of the exposure had an elongated shape, despite having almost similar stiffness (0.40 kPa) with hydrogel obtained through 15 min of the exposure (0.20 kPa) (Figure 6b–f). This phenomenon is similar to our previous report in human adipose-derived stem cells (hASCs) and rat fibroblast (3Y1) cells cultured on Gelatin–Ph hydrogel that showed elongated morphology on the hydrogel obtained through 60 min of exposure to H_2O_2 despite having similar stiffness with hydrogel obtained through 15 min of the exposure [31]. This phenomenon could be attributed to other factors such as mesoscale topographical changes and mesh size [67]. In the prolonged exposure time to H_2O_2, the phase-separation phenomenon might occur, resulting in the formation of a domain. Phase separation could be observed from the cloudy appearance of the fabricated hydrogel (Figure S10). This phase separation could induce clustering of cell surface receptors (see [68] for review), which could induce alteration of cell shape. Another factor that could induce better adhesion in the cells cultured on the hydrogel obtained through 120 min of the exposure is the low-molecular-weight fragments out of the polymer. As shown in Figure S9, H_2O_2 could degrade both Gelatin–Ph and HA–Ph. HA is well-known to have different modulatory effects based on their molecular weight [17–19]. Low-molecular-weight HA (LMW-HA) is reported to induce better adhesion in human epithelial cells HT1080, mediated by receptor for hyaluronic acid-mediated motility (RHAMM) [69]. LMW-HA also induces EGF-induced branching of mammary epithelial cells EpH4 and NMuMG cells, while the high-molecular-weight HA inhibits the morphological changes, a process that is mediated by HA receptors CD44 and RHAMM [70].

Another difference was found in the cell-cycle progression. Although HeLa/Fucci2 cells showed cell-cycle arrest at G2/M (Figure 4) in soft hydrogel obtained 15 min (0.20 kPa) and 120 min (0.40 kPa) of H_2O_2 exposure, NMuMG/Fucci2 cells showed an arrested cell-cycle at G1 phase (Figure 7). This difference was also reported in the previous report by Sakaue-Sawano et al. (2011), in which the cell type-dependent response is observed following exposure to Cdk4 inhibitor drugs, with HeLa/Fucci2 cells arrested at G2/M phase while NMuMG/Fucci2 cells are arrested at G1 phase [43]. At the moment, the intricate mechanism on how the H_2O_2 exposure time to Gelatin–Ph/HA–Ph hydrogel induced cell-cycle arrest at a different phase in HeLa/Fucci2 and NMuMG/Fucci2 is unknown. However, there is a possibility that NMuMG/Fucci2 cultured on Gelatin–Ph/HA–Ph hydrogel obtained through 120 min of the exposure had an epithelial-to-mesenchymal transition (EMT).

EMT is a physiological transition or reprogramming of epithelial cells to mesenchymal cells, marked by a morphological change into spindle-like mesenchymal cells, which plays an important role in the malignancy and invasiveness of cancer [44,45]. Recent study by Fan et al. (2021) shows that soft substrate (0.5 kPa) promotes the EMT in SKOV-3 ovarian cancer cells [71]. This stiffness is close with the Young's modulus of our Gelatin–Ph/HA–Ph hydrogel obtained through 120 min of H_2O_2-exposure at 0.40 kPa. Moreover, LMW-HA is also known to induce the EMT in MCF-7 and MDA-MB-231 cells [72]. This might explain why despite both Gelatin–Ph/HA–Ph composite hydrogel obtained through 15 min (0.20 kPa) and 120 min (0.40 kPa) of H_2O_2 exposure had low Young's modulus, but, the NMuMG/Fucci2 cells adhesion (Figure 6) and F-actin organization (Figure 8) were different: the molecular weight of HA–Ph exposed to H_2O_2 for 120 min was probably lower due to H_2O_2 degradation, which promotes EMT due to interaction with HA receptors such as CD44 or RHAMM.

As for the cell-cycle arrest in G1 observed in NMuMG/Fucci2 cells cultured on the hydrogel obtained through 120 min of H_2O_2 exposure (Figure 7), despite having similar F-actin organization with cells cultured on the hydrogel obtained through 60 min of H_2O_2 exposure (Figure 8), this could also be explained by the EMT process. EMT is known to induce cell-cycle arrest [73–75]. Additionally, *Snai1* and *Snai2* (Slug) which belong to

the SNAIL family transcription factors that regulate the EMT process are also known to regulate G1 phase transition [76].

Taken together, the contradictory effect of H_2O_2 to induce HRP-mediated cross-linking and degrade the Gelatin–Ph and HA–Ph polymer could affect the adhesion and cell-cycle progression of HeLa/Fucci2 and NMuMG/Fucci2 cells in cell type-dependent manner. These findings can be useful in biomedical field especially for creating tissues by combining cells and hydrogels obtained through HRP-mediated cross-linking. Development of various artificial tissues have been attempted by combining cells and the hydrogels for surgical transplantation and in vitro model for drug screening [77,78]. The control and understanding of the cell cycle in these engineered tissues are important for creating functional tissues and for accurately interpreting cellular responses to drug candidates, including anticancer drugs. Additionally, phenomenon reported in our study could be used to study the cancer cell behavior affected by the physicochemical property of their surrounding ECM. Future studies should be conducted to confirm the molecular mechanism of the cell-cycle regulation, adhesion, and also possibly EMT, by the mechanical property of the hydrogel and molecular weight of the polymer. Additionally, the adhesion and cell-cycle regulation of primary cancer cells on the composite hydrogel also needs to be investigated.

5. Conclusions

In this study, we investigated the H_2O_2 effect to induce HRP-mediated cross-linking and degrade polymer in Gelatin–Ph/HA–Ph composite hydrogel and its subsequent effect on cell adhesion and cell-cycle progression. Young's moduli of the Gelatin–Ph/HA–Ph composite hydrogels could be controlled by simple adjustment of the exposure time to H_2O_2 contained in the air, in which the stiffness increased after extending the exposure time from 15 to 60 min, followed by a decrease in extended exposure time to 120 min. The exposure time-dependent changes to the hydrogel stiffness governed the adhesion and cell-cycle progression of HeLa/Fucci2 cells and NMuMG/Fucci2 cells, in a cell-type-dependent manner. Although soft hydrogel leads to cell-cycle arrest at G2/M phase for HeLa/Fucci2, NMuMG/Fucci2 cells were arrested at G1 phase. Apart from hydrogel stiffness, the NMuMG/Fucci2 cell-cycle progression was also modulated by the H_2O_2-mediated degradation of HA in the composite, which produced low-molecular-weight HA. From these results, we conclude that the contradictory effects of H_2O_2 to Gelatin–Ph/HA–Ph composite hydrogel could be used to control the cell adhesion and cell-cycle progression, which could be used in cancer studies and tissue-engineering purposes.

Conflicts of Interest: The authors declare no conflict of interest.

References

1. Jingwen, B.; Yaochen, L.; Guojun, Z. Cell cycle regulation and anticancer drug discovery. *Cancer Biol. Med.* **2017**, *14*, 348–362. [CrossRef]
2. Stewart, Z.A.; Westfall, M.D.; Pietenpol, J.A. Cell-cycle dysregulation and anticancer therapy. *Trends Pharmacol. Sci.* **2003**, *24*, 139–145. [CrossRef]
3. Ni, Y.; Chiang, M.Y.M. Cell morphology and migration linked to substrate rigidity. *Soft Matter* **2007**, *3*, 1285–1292. [CrossRef]
4. Sun, M.; Chi, G.; Li, P.; Lv, S.; Xu, J.; Xu, Z.; Xia, Y.; Tan, Y.; Xu, J.; Li, L.; et al. Effects of Matrix Stiffness on the Morphology, Adhesion, Proliferation and Osteogenic Differentiation of Mesenchymal Stem Cells. *Int. J. Med. Sci.* **2018**, *15*, 257–268. [CrossRef]
5. Hadjipanayi, E.; Mudera, V.; Brown, R.A. Close dependence of fibroblast proliferation on collagen scaffold matrix stiffness. *J. Tissue Eng. Regen. Med.* **2009**, *3*, 77–84. [CrossRef]
6. Yeh, Y.-T.; Hur, S.S.; Chang, J.; Wang, K.-C.; Chiu, J.-J.; Li, Y.-S.; Chien, S. Matrix Stiffness Regulates Endothelial Cell Proliferation through Septin 9. *PLoS ONE* **2012**, *7*, e46889. [CrossRef]
7. Kalli, M.; Stylianopoulos, T. Defining the Role of Solid Stress and Matrix Stiffness in Cancer Cell Proliferation and Metastasis. *Front. Oncol.* **2018**, *8*, 55. [CrossRef]
8. Lebl, M.D.A.; Martins, J.R.M.; Nader, H.B.; Simões, M.D.J.; De Biase, N. Concentration and Distribution of Hyaluronic Acid in Human Vocal Folds. *Laryngoscope* **2007**, *117*, 595–599. [CrossRef]
9. Lee, S.-W.; Kim, J.; Do, M.J.; Namkoong, E.; Lee, H.; Ryu, J.H.; Park, K. Developmental role of hyaluronic acid and its application in salivary gland tissue engineering. *Acta Biomater.* **2020**, *115*, 275–287. [CrossRef]
10. Camci-Unal, G.; Cuttica, D.; Annabi, N.; Demarchi, D.; Khademhosseini, A. Synthesis and Characterization of Hybrid Hyaluronic Acid-Gelatin Hydrogels. *Biomacromolecules* **2013**, *14*, 1085–1092. [CrossRef]
11. Fraser, J.R.E.; Laurent, T.C.; Laurent, U.B.G. Hyaluronan: Its nature, distribution, functions and turnover. *J. Intern. Med.* **1997**, *242*, 27–33. [CrossRef] [PubMed]
12. Jiang, D.; Liang, J.; Noble, P.W. Hyaluronan in Tissue Injury and Repair. *Annu. Rev. Cell Dev. Biol.* **2007**, *23*, 435–461. [CrossRef]
13. Gómez-Guillén, M.; Giménez, B.; López-Caballero, M.; Montero, M. Functional and bioactive properties of collagen and gelatin from alternative sources: A review. *Food Hydrocoll.* **2011**, *25*, 1813–1827. [CrossRef]
14. Rezaeeyazdi, M.; Colombani, T.; Memic, A.; Bencherif, S.A. Injectable Hyaluronic Acid-co-Gelatin Cryogels for Tissue-Engineering Applications. *Materials* **2018**, *11*, 1374. [CrossRef] [PubMed]
15. Li, J.; He, A.; Zheng, J.; Han, C.C. Gelatin and Gelatin-Hyaluronic Acid Nanofibrous Membranes Produced by Electrospinning of Their Aqueous Solutions. *Biomacromolecules* **2006**, *7*, 2243–2247. [CrossRef]
16. Lam, T.; Dehne, T.; Krüger, J.P.; Hondke, S.; Endres, M.; Thomas, A.; Lauster, R.; Sittinger, M.; Kloke, L. Photopolymerizable gelatin and hyaluronic acid for stereolithographic 3D bioprinting of tissue-engineered cartilage. *J. Biomed. Mater. Res. Part. B Appl. Biomater.* **2019**, *107*, 2649–2657. [CrossRef]
17. Nyman, E.; Huss, F.; Nyman, T.; Junker, J.; Kratz, G. Hyaluronic acid, an important factor in the wound healing properties of amniotic fluid:In vitrostudies of re-epithelialisation in human skin wounds. *J. Plast. Surg. Hand Surg.* **2013**, *47*, 89–92. [CrossRef] [PubMed]
18. Termeer, C.; Benedix, F.; Sleeman, J.; Fieber, C.; Voith, U.; Ahrens, T.; Miyake, K.; Freudenberg, M.; Galanos, C.; Simon, J.C. Oligosaccharides of Hyaluronan Activate Dendritic Cells via Toll-like Receptor 4. *J. Exp. Med.* **2002**, *195*, 99–111. [CrossRef]

19. Termeer, C.C.; Hennies, J.; Voith, U.; Ahrens, T.; Weiss, J.; Prehm, P.; Simon, J.C. Oligosaccharides of Hyaluronan Are Potent Activators of Dendritic Cells. *J. Immunol.* **2000**, *165*, 1863–1870. [CrossRef] [PubMed]

20. Liu, M.; Tolg, C.; Turley, E. Dissecting the Dual Nature of Hyaluronan in the Tumor Microenvironment. *Front. Immunol.* **2019**, *10*, 947. [CrossRef] [PubMed]

21. Ooki, T.; Murata-Kamiya, N.; Kanemitsu, A.; Wu, W.; Hatakeyama, M. High-Molecular-Weight Hyaluronan Is a Hippo Pathway Ligand Directing Cell Density-Dependent Growth Inhibition via PAR1b. *Dev. Cell* **2019**, *49*, 590–604.e9. [CrossRef] [PubMed]

22. Fuchs, K.; Hippe, A.; Schmaus, A.; Homey, B.; Sleeman, J.; Orian-Rousseau, V. Opposing effects of high- and low-molecular weight hyaluronan on CXCL12-induced CXCR4 signaling depend on CD44. *Cell Death Dis.* **2013**, *4*, e819. [CrossRef]

23. Chen, H.; Qin, J.; Hu, Y. Efficient Degradation of High-Molecular-Weight Hyaluronic Acid by a Combination of Ultrasound, Hydrogen Peroxide, and Copper Ion. *Molecules* **2019**, *24*, 617. [CrossRef]

24. Liu, X.; Jiang, Y.; He, H.; Ping, W. Hydrogen peroxide-induced degradation of type I collagen fibers of tilapia skin. *Food Struct.* **2014**, *2*, 41–48. [CrossRef]

25. Li, X.; Xu, A.; Xie, H.; Yu, W.; Xie, W.; Ma, X. Preparation of low molecular weight alginate by hydrogen peroxide depolymerization for tissue engineering. *Carbohydr. Polym.* **2010**, *79*, 660–664. [CrossRef]

26. Chang, K.L.B.; Tai, M.-C.; Cheng, F.-H. Kinetics and Products of the Degradation of Chitosan by Hydrogen Peroxide. *J. Agric. Food Chem.* **2001**, *49*, 4845–4851. [CrossRef]

27. Park, J.; Baranov, P.; Aydin, A.; Abdelgawad, H.; Singh, D.; Niu, W.; Kurisawa, M.; Spector, M.; Young, M.J. In Situ Cross-linking Hydrogel as a Vehicle for Retinal Progenitor Cell Transplantation. *Cell Transplant.* **2019**, *28*, 596–606. [CrossRef]

28. Kondo, D.; Ogino, Y.; Ayukawa, Y.; Sakai, S.; Kawakami, K.; Koyano, K. Bone regeneration of tibial defects in rats with enzymatic hydrogelation of gelatin derivative and recombinant human platelet-derived growth factor-BB complex. *Int. J. Oral Maxillofac. Implant.* **2013**, *28*, 1377–1385. [CrossRef] [PubMed]

29. Yao, M.; Zhang, J.; Gao, F.; Chen, Y.; Ma, S.; Zhang, K.; Liu, H.; Guan, F. New BMSC-Laden Gelatin Hydrogel Formed in Situ by Dual-Enzymatic Cross-Linking Accelerates Dermal Wound Healing. *ACS Omega* **2019**, *4*, 8334–8340. [CrossRef]

30. Sakai, S.; Ueda, K.; Gantumur, E.; Taya, M.; Nakamura, M. Drop-On-Drop Multimaterial 3D Bioprinting Realized by Peroxidase-Mediated Cross-Linking. *Macromol. Rapid Commun.* **2017**, *39*. [CrossRef]

31. Mubarok, W.; Qu, Y.; Sakai, S. Influence of Hydrogen Peroxide-Mediated Cross-Linking and Degradation on Cell-Adhesive Gelatin Hydrogels. *ACS Appl. Bio Mater.* **2021**, *4*, 4184–4190. [CrossRef]

32. Gérard, C.; Goldbeter, A. The balance between cell cycle arrest and cell proliferation: Control by the extracellular matrix and by contact inhibition. *Interface Focus* **2014**, *4*, 20130075. [CrossRef] [PubMed]

33. Walker, C.; Mojares, E.; del Río Hernández, A. Role of Extracellular Matrix in Development and Cancer Progression. *Int. J. Mol. Sci.* **2018**, *19*, 3028. [CrossRef] [PubMed]

34. Greco, R.M.; Iocono, J.A.; Ehrlich, H.P. Hyaluronic acid stimulates human fibroblast proliferation within a collagen matrix. *J. Cell. Physiol.* **1998**, *177*, 465–473. [CrossRef]

35. Arya, A.D.; Hallur, P.M.; Karkisaval, A.G.; Gudipati, A.; Rajendiran, S.; Dhavale, V.; Ramachandran, B.; Jayaprakash, A.; Gundiah, N.; Chaubey, A. Gelatin Methacrylate Hydrogels as Biomimetic Three-Dimensional Matrixes for Modeling Breast Cancer Invasion and Chemoresponse in Vitro. *ACS Appl. Mater. Interfaces* **2016**, *8*, 22005–22017. [CrossRef] [PubMed]

36. Mao, J.S.; Cui, Y.L.; Wang, X.H.; Sun, Y.; Yin, Y.J.; Zhao, H.M.; De Yao, K. A preliminary study on chitosan and gelatin polyelectrolyte complex cytocompatibility by cell cycle and apoptosis analysis. *Biomaterials* **2004**, *25*, 3973–3981. [CrossRef] [PubMed]

37. Sheu, B.-C.; Lien, H.-C.; Ho, H.-N.; Lin, H.-H.; Chow, S.-N.; Huang, S.-C.; Hsu, S.-M. Increased expression and activation of gelatinolytic matrix metalloproteinases is associated with the progression and recurrence of human cervical cancer. *Cancer Res.* **2003**, *63*, 6537–6542. [PubMed]

38. Vu, M.; Yu, J.; Awolude, O.A.; Chuang, L. Cervical cancer worldwide. *Curr. Probl. Cancer* **2018**, *42*, 457–465. [CrossRef] [PubMed]

39. Canfell, K. Towards the global elimination of cervical cancer. *Papillomavirus Res.* **2019**, *8*, 100170. [CrossRef] [PubMed]

40. Qian, Q.; Wang, D.; Shi, L.; Zhang, Z.; Qian, J.; Shen, J.; Yu, C.; Zhu, X. A pure molecular drug hydrogel for post-surgical cancer treatment. *Biomaterials* **2020**, *265*, 120403. [CrossRef] [PubMed]

41. Lan, T.; Pang, J.; Wu, Y.; Zhu, M.; Yao, X.; Wu, M.; Qian, H.; Zhang, Z.; Gao, J.; Chen, Y. Cross-linked hyaluronic acid gel inhibits metastasis and growth of gastric and hepatic cancer cells: In vitro and in vivo studies. *Oncotarget* **2016**, *7*, 65418–65428. [CrossRef]

42. Ma, H.T.; Poon, R.Y.C. Synchronization of HeLa Cells. In *Methods in Molecular Biology (Methods and Protocols)*; Banfalvi, G., Ed.; Humana Press: New York, NY, USA, 2011; Volume 761, pp. 151–161. ISBN 978-1-61779-181-9.

43. Sakaue-Sawano, A.; Kobayashi, T.; Ohtawa, K.; Miyawaki, A. Drug-induced cell cycle modulation leading to cell-cycle arrest, nuclear mis-segregation, or endoreplication. *BMC Cell Biol.* **2011**, *12*, 2. [CrossRef]

44. Shin, S.; Buel, G.R.; Nagiec, M.J.; Han, M.-J.; Roux, P.P.; Blenis, J.; Yoon, S.-O. ERK2 regulates epithelial-to-mesenchymal plasticity through DOCK10-dependent Rac1/FoxO1 activation. *Proc. Natl. Acad. Sci. USA* **2019**, *116*, 2967–2976. [CrossRef]

45. Meyer-Schaller, N.; Cardner, M.; Diepenbruck, M.; Saxena, M.; Tiede, S.; Lüönd, F.; Ivanek, R.; Beerenwinkel, N.; Christofori, G. A Hierarchical Regulatory Landscape during the Multiple Stages of EMT. *Dev. Cell* **2019**, *48*, 539–553.e6. [CrossRef] [PubMed]

46. Sakai, S.; Hirose, K.; Taguchi, K.; Ogushi, Y.; Kawakami, K. An injectable, in situ enzymatically gellable, gelatin derivative for drug delivery and tissue engineering. *Biomaterials* **2009**, *30*, 3371–3377. [CrossRef] [PubMed]

47. Sakai, S.; Ueda, K.; Taya, M. Peritoneal adhesion prevention by a biodegradable hyaluronic acid-based hydrogel formed in situ through a cascade enzyme reaction initiated by contact with body fluid on tissue surfaces. *Acta Biomater.* **2015**, *24*, 152–158. [CrossRef] [PubMed]

48. Apraiz, A.; Mitxelena, J.; Zubiaga, A. Studying Cell Cycle-regulated Gene Expression by Two Complementary Cell Synchronization Protocols. *J. Vis. Exp.* **2017**. [CrossRef] [PubMed]

49. Sakai, S.; Ohi, H.; Taya, M. Gelatin/Hyaluronic Acid Content in Hydrogels Obtained through Blue Light-Induced Gelation Affects Hydrogel Properties and Adipose Stem Cell Behaviors. *Biomolecules* **2019**, *9*, 342. [CrossRef]

50. Matthews, H.K.; Bertoli, C.; de Bruin, R.A.M. Cell cycle control in cancer. *Nat. Rev. Mol. Cell Biol.* **2021**, *23*, 74–88. [CrossRef] [PubMed]

51. Schwartz, G.K.; Shah, M.A. Targeting the Cell Cycle: A New Approach to Cancer Therapy. *J. Clin. Oncol.* **2005**, *23*, 9408–9421. [CrossRef] [PubMed]

52. Baynton, K.J.; Bewtra, J.K.; Biswas, N.; Taylor, K.E. Inactivation of horseradish peroxidase by phenol and hydrogen peroxide: A kinetic investigation. *Biochim. Biophys. Acta (BBA) Protein Struct. Mol. Enzym.* **1994**, *1206*, 272–278. [CrossRef]

53. Arnao, M.; Acosta, M.; Del Rio, J.; Varón, R.; Garcia-Canovas, F. A kinetic study on the suicide inactivation of peroxidase by hydrogen peroxide. *Biochim. Biophys. Acta (BBA) Protein Struct. Mol. Enzym.* **1990**, *1041*, 43–47. [CrossRef]

54. Takahashi, S.; Itoh, N.; Kawamura, Y.; Hayashi, R. Physical and chemical changes of gelatins by oxidation treatment. *Bull. Soc. Sci. Photogr. Jpn.* **1998**, *51*, 22–28. (In Japanese) [CrossRef]

55. Fares, J.; Fares, M.Y.; Khachfe, H.H.; Salhab, H.A.; Fares, Y. Molecular principles of metastasis: A hallmark of cancer revisited. *Signal. Transduct. Target. Ther.* **2020**, *5*, 28. [CrossRef]

56. Ecker, B.L.; Kaur, A.; Douglass, S.M.; Webster, M.R.; Almeida, F.; Marino, G.; Sinnamon, A.J.; Neuwirth, M.G.; Alicea, G.M.; Ndoye, A.; et al. Age-Related Changes in HAPLN1 Increase Lymphatic Permeability and Affect Routes of Melanoma Metastasis. *Cancer Discov.* **2018**, *9*, 82–95. [CrossRef] [PubMed]

57. Nakahata, M.; Gantumur, E.; Furuno, K.; Sakai, S.; Taya, M. Versatility of hydrogelation by dual-enzymatic reactions with oxidases and peroxidase. *Biochem. Eng. J.* **2018**, *131*, 1–8. [CrossRef]

58. Le Thi, P.; Lee, Y.; Nguyen, D.H.; Park, K.D. In situ forming gelatin hydrogels by dual-enzymatic cross-linking for enhanced tissue adhesiveness. *J. Mater. Chem. B* **2016**, *5*, 757–764. [CrossRef] [PubMed]

59. Previtera, M.L.; Trout, K.; Verma, D.; Chippada, U.; Schloss, R.S.; Langrana, N.A. Fibroblast Morphology on Dynamic Softening of Hydrogels. *Ann. Biomed. Eng.* **2011**, *40*, 1061–1072. [CrossRef]

60. Paszek, M.J.; Zahir, N.; Johnson, K.R.; Lakins, J.N.; Rozenberg, G.I.; Gefen, A.; Reinhart-King, C.A.; Margulies, S.S.; Dembo, M.; Boettiger, D.; et al. Tensional homeostasis and the malignant phenotype. *Cancer Cell* **2005**, *8*, 241–254. [CrossRef]

61. Wall, S.J.; Zhong, Z.-D.; DeClerck, Y. The Cyclin-dependent Kinase Inhibitors p15INK4B and p21CIP1 Are Critical Regulators of Fibrillar Collagen-induced Tumor Cell Cycle Arrest. *J. Biol. Chem.* **2007**, *282*, 24471–24476. [CrossRef]

62. Klein, E.A.; Yin, L.; Kothapalli, D.; Castagnino, P.; Byfield, F.J.; Xu, T.; Levental, I.; Hawthorne, E.; Janmey, P.A.; Assoian, R.K. Cell-Cycle Control by Physiological Matrix Elasticity and In Vivo Tissue Stiffening. *Curr. Biol.* **2009**, *19*, 1511–1518. [CrossRef] [PubMed]

63. Kunda, P.; Baum, B. The actin cytoskeleton in spindle assembly and positioning. *Trends Cell Biol.* **2009**, *19*, 174–179. [CrossRef]

64. Reshetnikova, G.; Barkan, R.; Popov, B.; Nikolsky, N.; Chang, L.-S. Disruption of the Actin Cytoskeleton Leads to Inhibition of Mitogen-Induced Cyclin E Expression, Cdk2 Phosphorylation, and Nuclear Accumulation of the Retinoblastoma Protein-Related p107 Protein. *Exp. Cell Res.* **2000**, *259*, 35–53. [CrossRef] [PubMed]

65. An, W.G.; Shin, I.J.; Ahn, Y.-T.; Kim, Y.; Kim, J.-M. Actin disruption agents induce phosphorylation of histone H2AX in human breast adenocarcinoma MCF-7 cells. *Oncol. Rep.* **2011**, *25*, 1313–1319. [CrossRef] [PubMed]

66. Shrestha, D.; Choi, D.; Song, K. Actin Dysfunction Induces Cell Cycle Delay at G2/M with Sustained ERK and RSK Activation in IMR-90 Normal Human Fibroblasts. *Mol. Cells* **2018**, *41*, 436–443. [CrossRef]

67. Scott, R.A.; Robinson, K.G.; Kiick, K.L.; Akins, R.E. Human Adventitial Fibroblast Phenotype Depends on the Progression of Changes in Substrate Stiffness. *Adv. Heal. Mater.* **2020**, *9*, e1901593. [CrossRef]

68. Case, L.; Ditlev, J.A.; Rosen, M.K. Regulation of Transmembrane Signaling by Phase Separation. *Annu. Rev. Biophys.* **2019**, *48*, 465–494. [CrossRef]

69. Kouvidi, K.; Berdiaki, A.; Nikitovic, D.; Katonis, P.; Afratis, N.; Hascall, V.C.; Karamanos, N.; Tzanakakis, G. Role of Receptor for Hyaluronic Acid-mediated Motility (RHAMM) in Low Molecular Weight Hyaluronan (LMWHA)-mediated Fibrosarcoma Cell Adhesion. *J. Biol. Chem.* **2011**, *286*, 38509–38520. [CrossRef]

70. Tolg, C.; Yuan, H.; Flynn, S.M.; Basu, K.; Ma, J.; Tse, K.C.K.; Kowalska, B.; Vulkanesku, D.; Cowman, M.K.; McCarthy, J.B.; et al. Hyaluronan modulates growth factor induced mammary gland branching in a size dependent manner. *Matrix Biol.* **2017**, *63*, 117–132. [CrossRef] [PubMed]

71. Fan, Y.; Sun, Q.; Li, X.; Feng, J.; Ao, Z.; Li, X.; Wang, J. Substrate Stiffness Modulates the Growth, Phenotype, and Chemoresistance of Ovarian Cancer Cells. *Front. Cell Dev. Biol.* **2021**, *9*. [CrossRef] [PubMed]

72. Jariyal, H.; Gupta, C.; Srivastava, A. Hyaluronic acid induction on breast cancer stem cells unfolds subtype specific variations in stemness and epithelial-to-mesenchymal transition. *Int. J. Biol. Macromol.* **2020**, *160*, 1078–1089. [CrossRef]

73. Vega, S.; Morales, A.V.; Ocaña, O.H.; Valdés, F.; Fabregat, I.; Nieto, M.A. Snail blocks the cell cycle and confers resistance to cell death. *Genes Dev.* **2004**, *18*, 1131–1143. [CrossRef]

74. Prakash, V.; Carson, B.B.; Feenstra, J.M.; Dass, R.A.; Sekyrova, P.; Hoshino, A.; Petersen, J.; Guo, Y.; Parks, M.M.; Kurylo, C.M.; et al. Ribosome biogenesis during cell cycle arrest fuels EMT in development and disease. *Nat. Commun.* **2019**, *10*, 2110. [CrossRef]

75. Lovisa, S.; LeBleu, V.S.; Tampe, B.; Sugimoto, H.; Vadnagara, K.; Carstens, J.L.; Wu, C.-C.; Hagos, Y.; Burckhardt, B.C.; Pentcheva-Hoang, T.; et al. Epithelial-to-mesenchymal transition induces cell cycle arrest and parenchymal damage in renal fibrosis. *Nat. Med.* **2015**, *21*, 998–1009. [CrossRef]

76. Assani, G.; Zhou, Y. Effect of modulation of epithelial-mesenchymal transition regulators Snail1 and Snail2 on cancer cell radiosensitivity by targeting of the cell cycle, cell apoptosis and cell migration/invasion (Review). *Oncol. Lett.* **2018**, *17*, 23–30. [CrossRef]

77. Gantumur, E.; Kimura, M.; Taya, M.; Horie, M.; Nakamura, M.; Sakai, S. Inkjet micropatterning through horseradish peroxidase-mediated hydrogelation for controlled cell immobilization and microtissue fabrication. *Biofabrication* **2019**, *12*, 011001. [CrossRef]

78. Pierantoni, L.; Ribeiro, V.P.; Costa, L.; Pina, S.; Morais, A.D.S.; Silva-Correia, J.; Kundu, S.C.; Motta, A.; Reis, R.L.; Oliveira, J.M. Horseradish Peroxidase-Crosslinked Calcium-Containing Silk Fibroin Hydrogels as Artificial Matrices for Bone Cancer Research. *Macromol. Biosci.* **2021**, *21*, 2000425. [CrossRef]